# 3.1 DEVELOPMENT OF JMA'S NEW TURBULENCE INDEX

Atsushi Kudo *
Numerical Prediction Division
Japan Meteorological Agency, Tokyo, Japan

## 1. Introduction

In recent years, a large increase and congestion of air traffic are expected with increasing air transportation demand in Japan. Under the circumstances, it is the most important issue to maintain the safety of air transportation. Turbulence is one of the most hazardous weather for safety flight. According to the statistics of Japan Transport Safety Board between 2000 and 2009, about half of airliner accidents are caused by turbulence in Japan. Accurate turbulence forecast is necessary to reduce the risk of turbulence.

Japan Meteorological Agency (JMA) has responsibility for Fukuoka FIR which is one of the most turbulence prone regions in the world. Maximum wind speeds in jet streams sometimes exceed 200 kt in winter, which causes clear air turbulence (CAT); strong seasonal winds and complex terrain cause mountain waves and wind shears; the Meiyu–Baiu fronts form during early summer and typhoons strike in summer and autumn, causing turbulence associated with clouds.

JMA have been mainly used vertical wind shear (VWS) as a turbulence forecast index. Although VWS is a simple index, our verifications intended for the area around Japan (Obayashi and Sakakibara 2000, Kudo 2008, Yamada 2008) show that the forecast accuracy is the same or more than other widely used indices, e.g. Ellrod indices (TI1, TI2) (Ellrod and Knapp 1992), Dutton's empirical index (DI) (Dutton 1980), Richardson number (Ri), horizontal wind shear (HWS), and horizontal temperature gradient (TEMPG). However, the accuracy is still insufficient.

There are two reasons why VWS is insufficient for turbulence forecast. One reason is that VWS is inadequate to predict turbulences unrelated to Kelvin-Helmholtz (KH) instability (e.g., Browning et al. 1973; Lilly 1986; Fritts et al. 2003). Although KH instability is one of the main causes of turbulence, turbulence is caused by various reasons. For example, turbulence in or around convective clouds (e.g., MacCready 1964; MacPherson and Isaac 1977, Lane and Sharman 2008; Trier et al. 2010), turbulence arise from mountain waves and other internal gravity waves (Scorer 1949; McCann 2001; Knox 1997), turbulence beneath the mid-level cloud bases (Kudo 2011), and turbulence associated with transverse band clouds (Oono and Miura 1982; Knox et al. 2010) can occur independently of KH instability. Thus, it is inadequate to predict these turbulences by using VWS. Another reason is that even if the turbulence is caused by KH instability, forecast can be insufficient owing to the insufficient resolution of numerical weather prediction (NWP) models. It is said that the scale of turbulence affect large aircraft is about between several tens of meters and 1 or 2 kilometers, the current mesoscale model (MSM) operated in JMA (Saito et al. 2006, 2007) whose horizontal grid interval is 5 km cannot directory resolve the turbulence.

Many indices are proposed to predict turbulence, but as described above, the accuracy is not better significantly compared with VWS in our verifications. In order to predict turbulence accurately, the index should be the one which can forecast both turbulence via KH instability as with VWS and turbulence via non-KH instability. In the United States, the Graphical Turbulence Guidance (GTG) system which is a weighted ensemble of turbulence indices was developed and has operated (Sharman et al. 2006). The verification shows that the forecast accuracy is better compared with every individual index used in GTG. In JMA, Yamada (2008) developed a turbulence probability guidance which is an index that combines multiple turbulence indices for CAT, lee waves and convective clouds by using decision tree. The verification shows that the turbulence probability has the same or better

* *Corresponding author address:* Atsushi Kudo, Numerical Prediction Division, Japan Meteorological Agency, Chiyoda, Tokyo 100-8122, Japan. E-mail: kudo@met.kishou.go.jp

Table 1. Correlation coefficients at FL130. Coefficients those are 1.0－0.6, 0.6－0.4, and 0.4－0.0 are highlighted by red, yellow, and blue, respectively.

| | SWS | MTW1 | MTW2 | BASETB | TRAV | CONV | VWS | HWS | RI | TEMPG | TI1 | TI2 | DI | TPI | TSI |
|---|---|---|---|---|---|---|---|---|---|---|---|---|---|---|---|
| SWS | 1.00 | 0.02 | 0.04 | 0.08 | −0.02 | 0.15 | 0.89 | 0.64 | −0.54 | 0.58 | 0.83 | 0.81 | 0.90 | 0.60 | 0.14 |
| MTW1 | 0.02 | 1.00 | 0.02 | −0.01 | 0.00 | −0.01 | −0.02 | 0.06 | 0.00 | 0.02 | 0.09 | 0.08 | −0.01 | 0.03 | 0.02 |
| MTW2 | 0.04 | 0.02 | 1.00 | 0.00 | 0.00 | 0.03 | −0.01 | 0.11 | −0.01 | 0.01 | 0.17 | 0.17 | 0.00 | 0.00 | −0.02 |
| BASETB | 0.08 | −0.01 | 0.00 | 1.00 | 0.00 | −0.03 | 0.05 | 0.14 | −0.05 | 0.01 | 0.32 | 0.31 | 0.06 | 0.03 | −0.01 |
| TRAV | −0.02 | 0.00 | 0.00 | 0.00 | 1.00 | 0.00 | −0.01 | −0.01 | −0.01 | −0.01 | −0.02 | −0.02 | −0.01 | 0.00 | 0.00 |
| CONV | 0.15 | −0.01 | 0.03 | −0.03 | 0.00 | 1.00 | 0.07 | 0.24 | −0.06 | 0.04 | 0.28 | 0.27 | 0.09 | 0.18 | −0.16 |
| VWS | 0.89 | −0.02 | −0.01 | 0.05 | −0.01 | 0.07 | 1.00 | 0.35 | −0.64 | 0.58 | 0.73 | 0.71 | 0.93 | 0.56 | 0.14 |
| HWS | 0.64 | 0.06 | 0.11 | 0.14 | −0.01 | 0.24 | 0.35 | 1.00 | −0.19 | 0.34 | 0.60 | 0.58 | 0.52 | 0.48 | 0.07 |
| RI | −0.54 | 0.00 | −0.01 | −0.05 | −0.01 | −0.06 | −0.64 | −0.19 | 1.00 | −0.31 | −0.45 | −0.43 | −0.43 | −0.28 | −0.07 |
| GRADT | 0.58 | 0.02 | 0.01 | 0.01 | −0.01 | 0.04 | 0.58 | 0.34 | −0.31 | 1.00 | 0.52 | 0.51 | 0.60 | 0.50 | 0.19 |
| TI1 | 0.83 | 0.09 | 0.17 | 0.32 | −0.02 | 0.28 | 0.73 | 0.60 | −0.45 | 0.52 | 1.00 | 0.99 | 0.74 | 0.54 | −0.01 |
| TI2 | 0.81 | 0.08 | 0.17 | 0.31 | −0.02 | 0.27 | 0.71 | 0.58 | −0.43 | 0.51 | 0.99 | 1.00 | 0.72 | 0.52 | −0.01 |
| DI | 0.90 | −0.01 | 0.00 | 0.06 | −0.01 | 0.09 | 0.93 | 0.52 | −0.43 | 0.60 | 0.74 | 0.72 | 1.00 | 0.63 | 0.15 |
| TPI | 0.60 | 0.03 | 0.00 | 0.03 | 0.00 | 0.18 | 0.56 | 0.48 | −0.28 | 0.50 | 0.54 | 0.52 | 0.63 | 1.00 | 0.12 |
| TSI | 0.14 | 0.02 | −0.02 | −0.01 | 0.00 | −0.16 | 0.14 | 0.07 | −0.07 | 0.19 | −0.01 | −0.01 | 0.15 | 0.12 | 1.00 |

accuracy compared with VWS, Ri, TI1, and TI2.

The idea of combining multiple indices is reasonable because turbulence is caused by various reasons. By combining multiple indices, the forecast accuracy is expected to be better as shown in GTG.

In accord with the above, a new turbulence index which is called TBindex was developed. It is confirmed through verification results that TBindex improves forecast accuracy significantly compared to VWS or other conventional indices. TBindex has been in operation in JMA since March 2011, and utilized as one of basic data for issuance of SIGMET and the domestic significant weather prognostic chart.

In the next section, the making procedure for TBindex is given. Verification results and case studies are shown in section 3 and 4 respectively. Summary and conclusion are presented in the last section.

## 2. Making procedure

### *2.1 Basic ideas for TBindex*

TBindex is a combined index of multiple turbulence indices derived from NWP models as with GTG and Yamada (2008). TBindex uses logistic regression method for the way to combine multiple indices while GTG uses weighted ensemble and Yamada (2008) uses decision tree. This is because the objective variable used here is pilot reports (PIREP) which is a binary of "turbulence" or "non-turbulence", and logistic regression is appropriate for binary variables. Sharman et al. (2006) shows that if the training data is enough, the performance of GTG and that of logistic regression become very close.

TBindex intends to predict various kinds of turbulence, i.e. CAT, mountain waves and cloud related turbulences, over all height. To achieve this, indices for non-CAT turbulence need to be added to the explanatory variables. However, few indices are proposed for non-CAT turbulence. Therefore some diagnostics for mainly non-CAT turbulence are newly developed, and then these diagnostics and existing CAT indices are combined by logistic regression method. The new diagnostics developed here are skew wind shear (SWS), convective cloud turbulence index (CONV), lee wave turbulence index (MTW1), vertically propagating mountain wave turbulence index (MTW2), mid-level cloud-base turbulence index (BASETB), and transverse band index (TRAV). Specifics for these newly developed indices are summarized in Appendix A. Fifteen indices are prepared for candidates of explanatory variables in this study, which is SWS, CONV, MTW1, MTW2, BASETB, TRAV, VWS, HWS, Ri, TEMPG, TI1, TI2, DI, and Miyakoshi's indices (TPI, TSI) (Miyakoshi 2003). TBindex and all explanatory variables are calculated in 40 km horizontal grid and 2000 ft vertical grid based on MSM model output.

### *2.2 Select independent indices*

For making TBindex, not all candidates shown in the previous section but only independent indices are selected and used. By selecting independent indices, operators become easy to understand which indices contribute to TBindex.

To study independence of each index, correlation coefficients between two indices are calculated. For example, that in FL130 are

Table 2. Regression coefficients for each level. The coefficients are multiplied by typical values in order to facilitate the comparison. Absolute values those are greater than 0.5 are highlighted by blue.

| | intercept | SWS | CONV | TSI | TPI | TEMPG | RI | MTW1 | BASETB | MTW2 | TRAV |
|---|---|---|---|---|---|---|---|---|---|---|---|
| FL410 | −7.26 | 3.08 | 0.78 | 0.22 | | | | | | | 0.65 |
| FL390 | −7.13 | 2.93 | 0.73 | 0.15 | 0.10 | | | | | | 0.53 |
| FL370 | −6.87 | 2.71 | 1.06 | 0.09 | 0.10 | | | | | | 0.35 |
| FL350 | −6.81 | 2.88 | 1.04 | 0.10 | 0.14 | | | | | | |
| FL330 | −6.67 | 3.06 | 1.26 | 0.17 | 0.13 | | 0.04 | | | | 0.14 |
| FL310 | −6.59 | 3.02 | 1.33 | 0.08 | 0.16 | | 0.04 | | | 0.66 | |
| FL290 | −6.71 | 3.07 | 1.50 | | 0.18 | | | | | | 0.22 |
| FL270 | −6.48 | 2.91 | 1.59 | 0.06 | 0.20 | | −0.08 | | | 0.40 | 0.39 |
| FL250 | −6.32 | 2.82 | 1.37 | 0.12 | 0.21 | | −0.05 | | 2.04 | 0.88 | 0.32 |
| FL230 | −6.39 | 3.06 | 1.21 | 0.09 | 0.23 | | | | 1.93 | 1.12 | 0.42 |
| FL210 | −6.28 | 3.48 | 1.15 | | 0.21 | −0.16 | | | 1.59 | 1.10 | 0.78 |
| FL190 | −6.14 | 3.54 | 0.94 | −0.14 | 0.15 | −0.13 | 0.07 | | 1.44 | 1.17 | 0.79 |
| FL170 | −5.90 | 3.19 | 0.95 | −0.40 | 0.10 | 0.10 | 0.06 | 0.51 | 1.68 | 0.94 | |
| FL150 | −5.49 | 2.94 | 1.04 | −0.42 | 0.13 | 0.28 | 0.06 | 0.78 | 1.74 | 0.83 | |
| FL130 | −4.81 | 2.59 | 0.89 | −0.45 | 0.29 | 0.24 | | 0.63 | 1.45 | 1.45 | |
| FL110 | −4.68 | 2.53 | 0.71 | −0.39 | 0.32 | 0.26 | | 0.60 | 1.16 | 1.41 | |
| FL090 | −4.66 | 2.48 | 0.43 | | 0.50 | 0.29 | 0.06 | 0.59 | 0.73 | 1.07 | |
| FL070 | −4.73 | 2.51 | 0.36 | −0.33 | 0.54 | 0.28 | | 0.72 | | | |
| FL050 | −4.62 | 2.23 | 0.30 | −0.84 | 0.23 | 0.26 | −0.06 | 0.78 | | | |
| FL030 | −4.50 | 2.10 | | −1.11 | | | | 0.62 | | | |

shown in Table 1 in which a strong (1.0－0.6), moderate (0.6－0.4), and weak (0.4 － 0.0) correlation are highlighted by red, yellow and blue, respectively. As shown in Table 1, the correlation coefficients of MTW1, MTW2, BASETB, TRAV, CONV, and TSI are small for every index, which means these indices are independent. On the other hand, VWS, HWS, Ri, TEMPG, TI1, TI2, DI, and TPI, these are indices intended for CAT, have a moderate to strong correlation with SWS.

By calculating correlation coefficients for every level, it is found that VWS, HWS, TI1, TI2, and DI have a strong correlation with SWS for most levels. Therefore only SWS is selected for explanatory variables due to the forecast accuracy (see Appendix A). The other candidates with moderate correlation are used as explanatory variables. Finally, ten indices, i.e. SWS, MTW1, MTW2, BASETB, TRAV, CONV, Ri, TEMPG, TPI, and TSI are selected.

### *2.3 Logistic regression method*

As making regression equations, adequate indices are selected from among the ten indices based on Akaike's information criterion which estimates a goodness of statistical models. Common-PIREP (C-PIREP) (Nakazawa 2003) is used as the objective variable where moderate or greater turbulence (MOG) reports are treated as 1 and the others are treated as 0. Every C-PIREP is reported by Japanese commercial airliners, which means almost every C-PIREP is reported by large aircraft. The training data is two years from January 2008 to December 2009. In this period, approximately 1.8 million C-PIREPs include approximately 16 thousand (0.89%) C-PIREPs of MOG turbulence are reported. Regression equations are stratified by altitudes because a cause of turbulence varies with altitudes. Specifically, the equations are stratified in 2000 ft intervals from FL030 to FL410. Owing to the small observation below FL010 and above FL430, the equation for FL030 is used for FL010 and the equation for FL410 is used for FL430 or above.

Table 2 shows the regression coefficients for each level, where the coefficients are multiplied by typical values in order to facilitate the comparison. Because the typical values vary with altitudes in general, we cannot compare

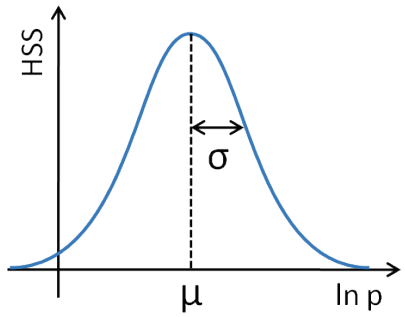


Fig. 1. A pattern diagram for adjusting the index. A standard deviation σ and a threshold μ which maximize HSS.

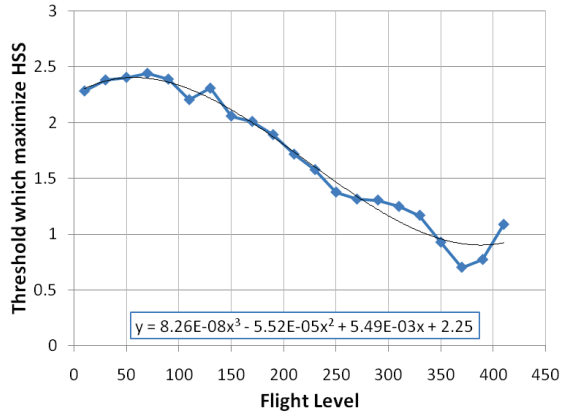


Fig. 2. Thresholds which maximize HSS for each flight level and the approximate equation.

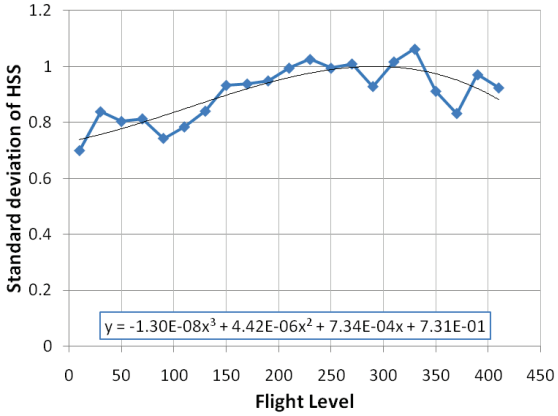


Fig. 3. Standard deviations of HSS for each flight level and the approximate equation.

exactly, but if the absolute values in Table 2 is large, the contribution to TBindex will be large. Blanks present that the index is rejected at the altitude, that is, the coefficient is zero. Values those are greater than 0.5 are highlighted by blue in the table. As shown in Table 2, SWS has the largest contribution to TBindex in all levels except for intercept terms. CONV is also adopted at most levels and the contributions are relatively large. MTW1 is adopted in lower to middle levels, MTW2 and BASETB are adopted in middle levels. Their contributions are also relatively large. In contrast, the contributions of TSI, TPI, TEMPG, Ri, and TRAV are relatively small in most levels.

### *2.4 Adjustment of the index*

In logistic regression, the objective variable is a log odds ratio of event. Therefore the value x calculated by the regression equation in the previous section presents a probability of turbulence p (%) through the following relation.

$$p = 100 \times e^x/(1 + e^x)$$

Turbulence probability forecast is useful for users but the probability calculated here is not a probability in the real sense because the turbulence distribution derived from C-PIREP which is used as the objective variable does not present the real distribution. Thus, it is inadequate to use the value p as a probability of turbulence. Meanwhile, it is inadequate for operators to use the value p directly because appropriate thresholds vary with altitudes in general. Therefore, operators have to change the threshold in response to the altitude if they attempt to make the optimum forecast. For these reasons, instead of using the probability value p directly, p is adjusted to be able to predict turbulence optimally at the same threshold in every altitude. The adjusted value becomes TBindex. Data used for the adjustment is the same period as making the regression equations.

First, the probability value p derived from the regression equations is taken the logarithm to smoothen the changes. Next, a distribution of Heidke Skill Score (HSS) (see Appendix B) is derived for each altitude and various thresholds of ln p, and then the standard deviation σ and a threshold μ which maximizes HSS are estimated (a pattern diagram is shown in Fig. 1). Figure 2 and 3 show μ and σ at each altitude and their

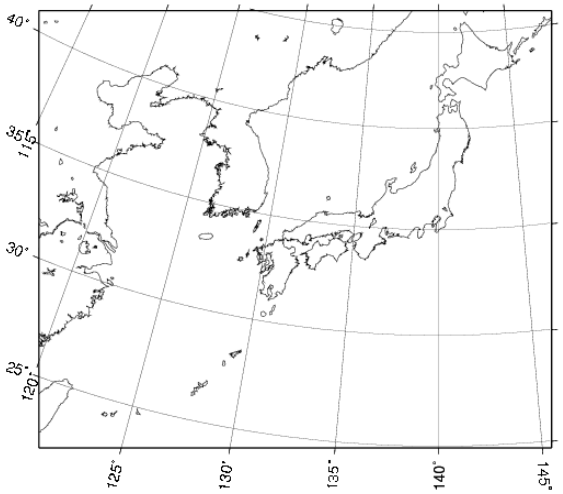


Fig. 4. Verification and calculation region of TBindex.

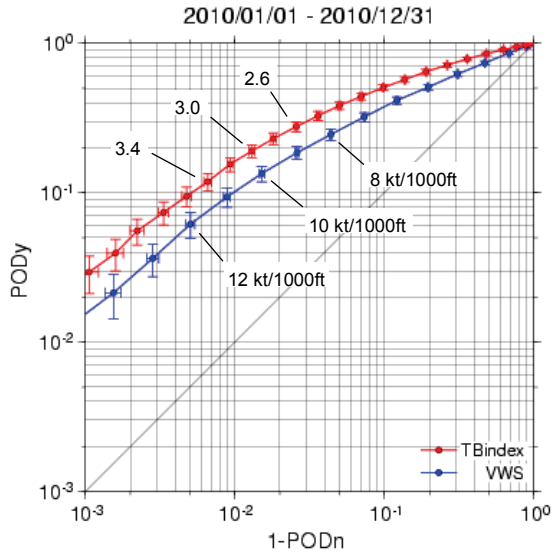


Fig. 5. PODy-PODn performance statistics for MOG turbulence. The error bars indicate 95 % confidence interval.

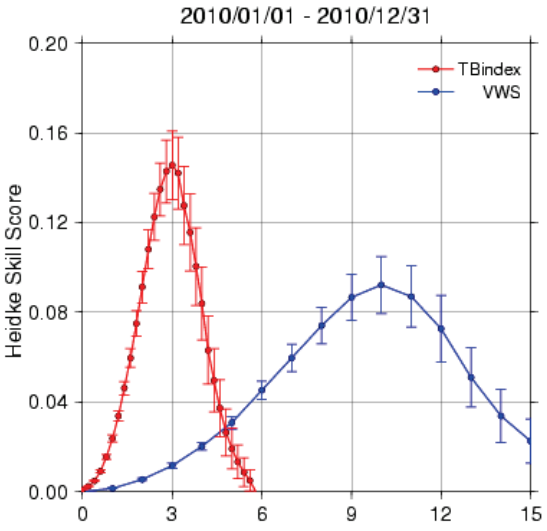


Fig. 6. HSS for MOG turbulence. The horizontal axis indicates TBindex and VWS (kt/1000ft). The error bars indicate 95 % confidence interval.

approximate equation respectively. TBindex is defined as a value with the mean value and the standard deviation for the distribution of HSS equals 3.0 and 1.0, respectively. The equation can be written as follows:

$$\mathrm{TBindex} = \frac{\ln p - \mu}{\sigma} + 3.0$$

By adding 3.0, most TBindex is adjusted to a positive value. The forecast accuracy is exactly the same before and after adding 3.0. By adjusting the index in this way, operators will be able to predict turbulence optimally at the same threshold (TBindex=3.0) in every altitude.

## 3. Verification

The performance of TBindex is shown in this section. In order to compare the forecast accuracy, the verification results of VWS is also shown. Verification data used here is one year from January to December 2010 which is independent on the training data. TBindex and VWS are calculated in 40 km horizontal interval and 2000 ft vertical interval from FL010 to FL550 in 1-hour forecast time interval in a region shown in Fig. 4. Observation data used here is C-PIREP. In the verification period, approximately 930 thousand C-PIREPs include approximately 8.6 thousand (0.92%) C-PIREPs of MOG turbulence are reported. Every report is distributed to the nearest forecast grid and time, and compared with the forecast.

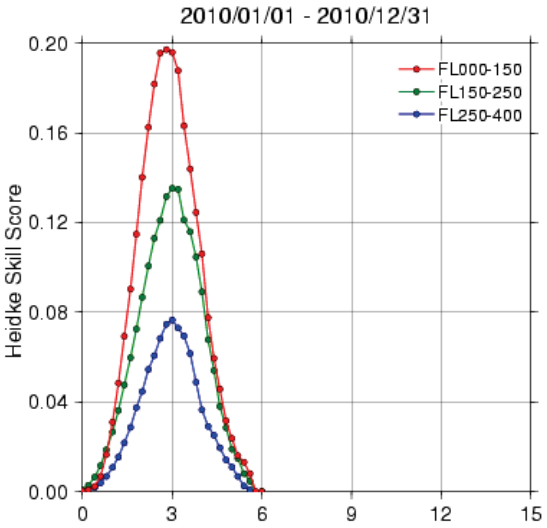


Fig. 7. HSS for MOG turbulence according to altitudes and thresholds.

Figure 5 shows PODy-PODn (see Appendix B) performance statistics for MOG turbulence. Verification results of forecast time from FT=4 to 15 and all forecast altitude are summed up in Fig. 5. In the PODy-PODn diagram, lines located on near the upper-left corner have a good performance. As shown in Fig. 5, the forecast accuracy of TBindex surpasses VWS

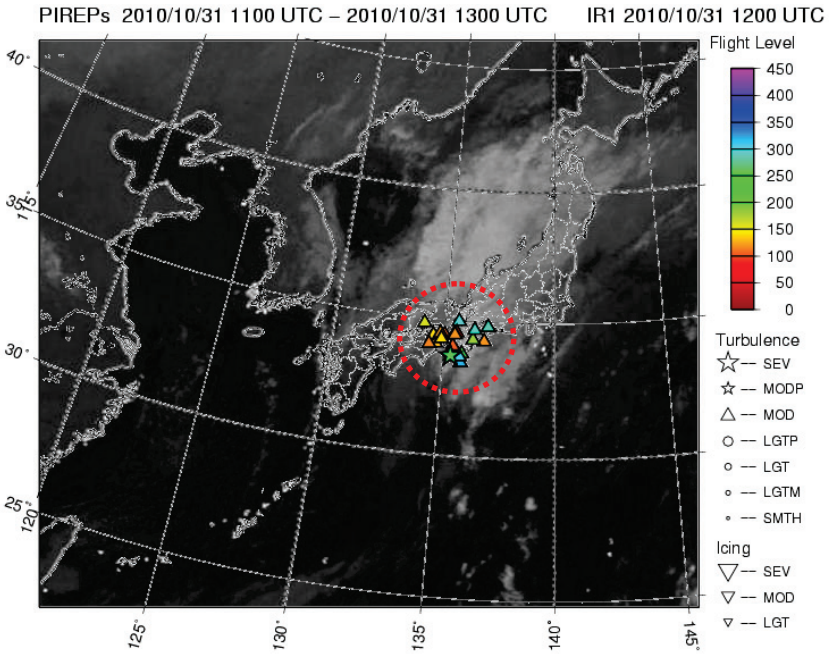


Fig. 8. IR imagery at 12 UTC 31 Oct 2010 and turbulence observed between 11 and 13 UTC. Only MOG turbulence is depicted. Symbols indicate the intensity and the color indicates the flight level.

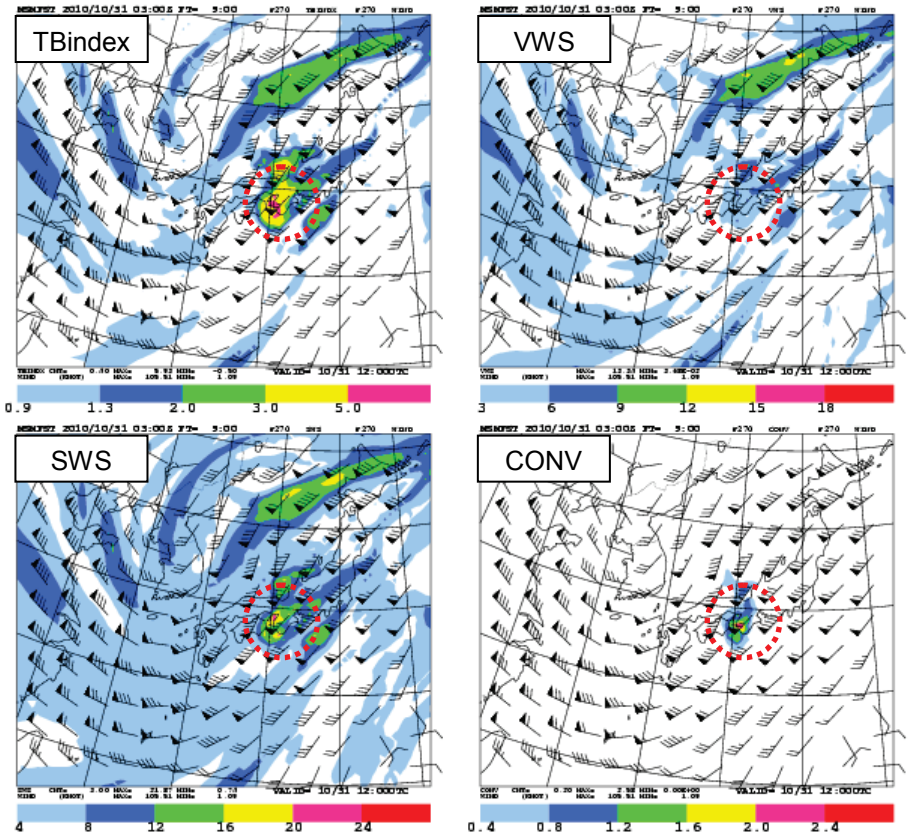


Fig. 9. 9-hour forecast of TBindex, VWS, SWS, and CONV at FL270 based at 03 UTC 31 Oct 2010.

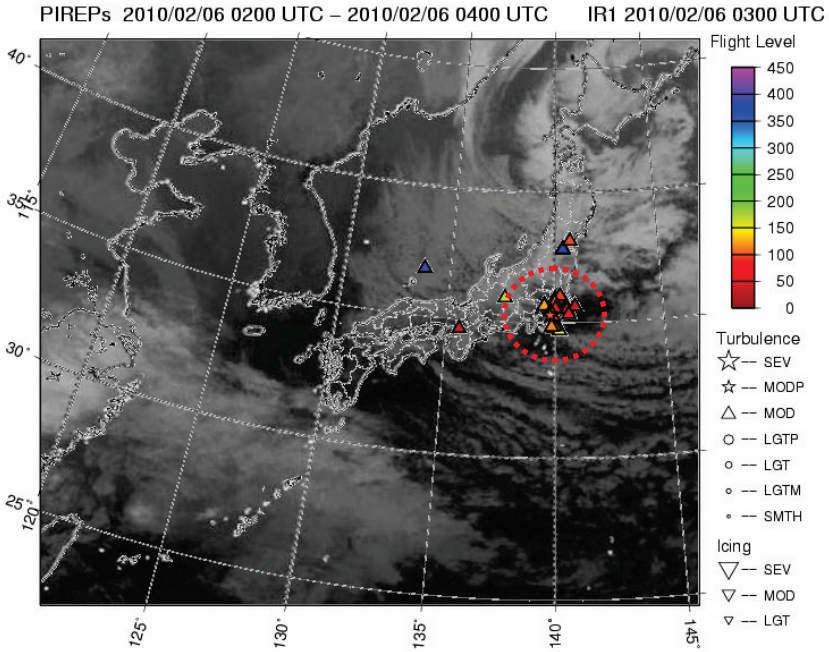


Fig. 10. IR imagery at 03 UTC 6 Feb 2010 and turbulence observed between 02 and 04 UTC. Only MOG turbulence is depicted. Symbols indicate the intensity and the color indicates the flight level.

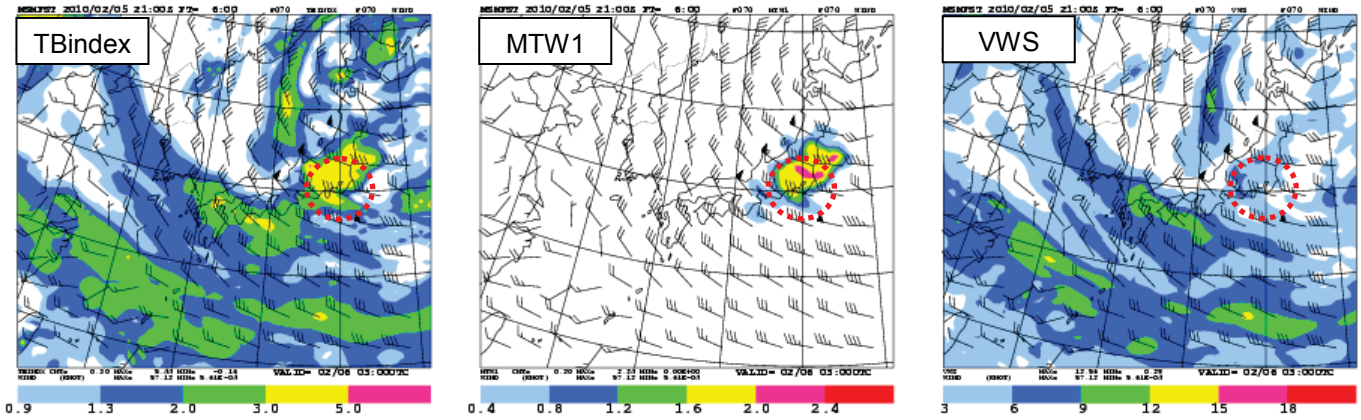


Fig. 11. 6-hour forecast of TBindex, MTW1, and VWS at FL070 based at 21 UTC 5 Feb 2010.

significantly.

Figure 6 shows HSS for TBindex and VWS, where the verification condition is the same as Fig. 5. The maximum HSS appears at TBindex=3.0, which indicates that the adjustment works as intended. The maximum HSS value of TBindex exceeds that of VWS significantly, which indicates the forecast accuracy of TBindex surpasses VWS significantly.

Figure 7 shows HSS for TBindex according to altitudes and thresholds. HSS become maximum at about TBindex=3.0 in every altitude. That means, the adjustment works well as intended and TBindex=3.0 is the optimal threshold for MOG turbulence regardless of altitude.

## 4. Case study

Three cases in which turbulence occur frequently without strong VWS are shown in this section. Cases with strong VWS are not shown here but if VWS is strong, SWS is strong too, which makes TBindex large.

### *Case 1. Turbulence in and top of convective clouds*

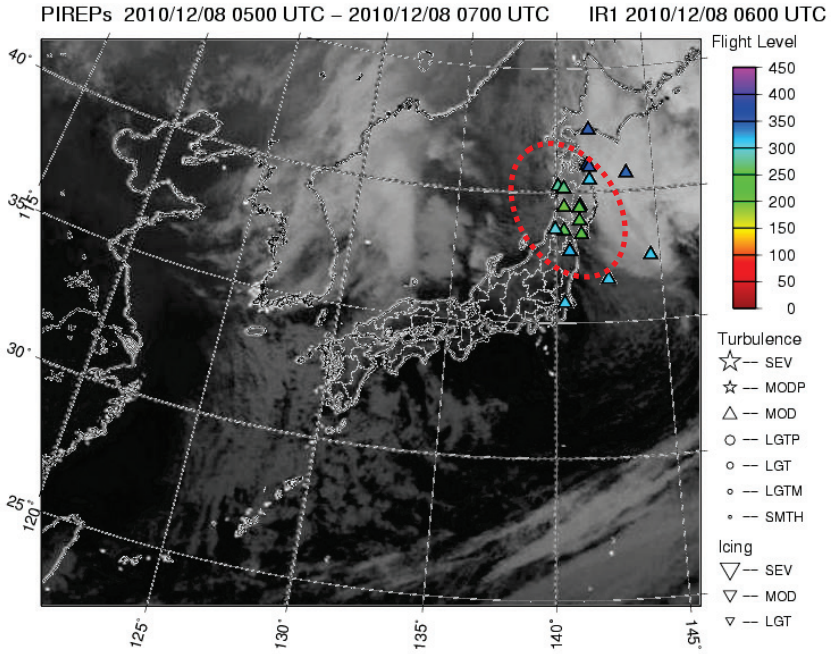


Fig. 12. IR imagery at 06 UTC 8 Dec 2010 and turbulence observed between 05 and 07 UTC. Only MOG turbulence is depicted. Symbols indicate the intensity and the color indicates the flight level.

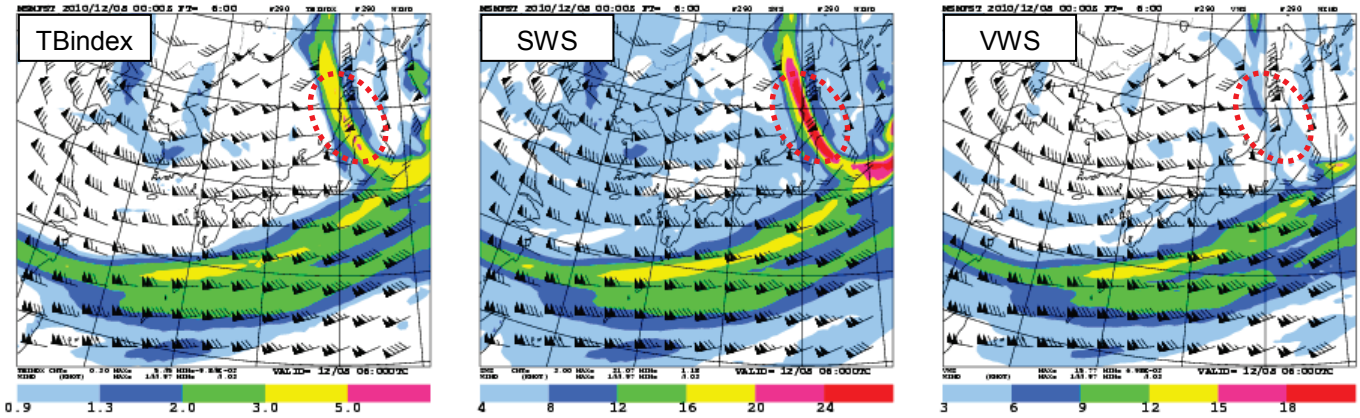


Fig. 13. 6-hour forecast of TBindex, SWS, and VWS at FL290 based at 00 UTC 8 Dec 2010.

Around 12 UTC (21 JST) 31 Oct 2010, large number of MOG turbulences were reported around the Kii peninsula (red dotted circle area in Fig. 8). Figure 8 shows a composite of IR imagery at 12 UTC and MOG turbulences reported between 11 and 13 UTC. A low pressure system was located off the south coast of the Kii peninsula at 12 UTC (data not shown), and associated cloud band spread toward the north direction. Turbulences occurred in and top of the cloud band between FL100 and FL370. Severe turbulence occurred between FL250 and FL270. Figure 9 shows 9-hour forecast of TBindex, VWS, SWS, and CONV at FL270 based at 03 UTC 31 Oct 2010. VWS is small (3 ～6 kt/1000ft) in the area of severe turbulence, but TBindex is large (the maximum value is greater than 5.0) because of large SWS and CONV.

### *Case 2. Turbulence arise from lee wave*

Around 03 UTC (12 JST) 6 Feb 2010, large number of MOG turbulences were reported over the Kanto plain (red dotted circle area in Fig. 10). Figure 10 shows a composite of IR imagery at 03 UTC and MOG turbulences reported between 02 and 04 UTC. Cloud streets with cold outbreak

were found in the Sea of Japan and the Pacific, which indicates that strong northwesterly seasonal wind blows in the lower layer. That causes lee waves and associated turbulences in the lee of the Chubu Mountain Range which is located in the north to west of the Kanto plain. Turbulences occurred below FL140. Figure 11 shows 6-hour forecast of TBindex, MTW1, and VWS at FL070 based at 21 UTC 5 Feb 2010. VWS is small (3～6 kt/1000ft) in the area of turbulence, but TBindex is large (the maximum value is greater than 3.0) because of large MTW1.

***Case 3. Clear air turbulence***

Around 06 UTC (15 JST) 8 Dec 2010, large number of moderate turbulences were reported over the Tohoku district (red dotted circle area in Fig 12). Figure 12 shows a composite of IR imagery at 06 UTC and MOG turbulences reported between 05 and 07 UTC. A number of moderate turbulences reported between FL240 and FL340 around a trough with a convective outflow boundary. Figure 13 shows 6-hour forecast of TBindex, SWS, and VWS at FL290 based at 00 UTC 8 Dec 2010. VWS is small (3～6 kt/1000ft) in the area of turbulence, but TBindex is large because of large SWS.

## 5. Summary and conclusion

A new turbulence forecast index (TBindex) was developed, which is a combination of newly developed diagnostics for mainly non-CAT turbulences and existing turbulence indices using logistic regression method. By using only independent indices for explanatory variables, operators can easily understand which indices contribute to TBindex. In addition, by adjusting the index, TBindex can predict turbulence optimally at the same threshold regardless of altitude.

Statistical verification and case studies show that the forecast accuracy of TBindex surpasses VWS significantly. TBindex can forecast various kinds of turbulence over all height in a comprehensive manner.

TBindex has been in operation in JMA since March 2011, and utilized as one of basic data for issuance of SIGMET and the domestic significant weather prognostic chart.

## References


Browning, K. A., G.W. Bryant, J. R. Starr, and D. N. Axford 1973: Air motion within Kelvin-Helmholtz billows determined from simultaneous Doppler radar and aircraft measurements. Quart. J. Roy. Meteor. Soc., 99, 608-618.

Dutton, M. J. O., 1980: Probability forecasts of clear-air turbulence based on NWP model output, Meteorological Magazine, 109, 293-310.

Ellrod, G. P. and D. I. Knapp, 1992: An Objective Clear-Air Turbulence Forecasting Technique: Verification and Operational Use, Weather and Forecasting, 7, 150-165.

Fritts, D. C., C. Bizon, J. A. Werne, and C. K. Meyer, 2003: Layering accompanying turbulence generation due to shear instability and gravity-wave breaking. J. Geophys. Res., 108(D8), 8452, doi:10.1029/2002JD002406.

Gerbier, N. and M. Berenger, 1961: Experimental studies of lee waves in the French Alps. Quart. J. Roy. Meteor. Soc. 87, 13-23.

Knox, J. A., 1997: Possible Mechanisms of Clear-Air Turbulence in Strongly Anticyclonic Flows, Mon. Wea. Rev., 125, 1251-1259.

Knox, J. A., A. S. Bachmeier, W. M. Carter, J. E. Tarantino, L. C. Paulik, E. N. Wilson, G. S. Bechdol, and M. J. Mays, 2010: Transverse cirrus bands in weather systems: a grand tour of an enduring enigma, Weather 65, 35-41.

Kudo, A. 2008: Significant weather GPV for domestic area forecast. Text for NWP-training (*in Japanese, Suuchiyohou Kenshu Text*), Japan Meteorological Agency, 92-98.

Kudo, A. 2011: Formation mechanisms of turbulence beneath the mid-level cloud base: The effect of sublimation cooling of snow. submitted to J. Appl. Meteor. Clim.

Lane, T. P., and R. D. Sharman, 2008: Some Influences of Background Flow Conditions on the Generation of Turbulence due to Gravity Wave Breaking above Deep Convection. J. Appl.

Meteor. Clim., 47, 2777-2796.

Lilly, D. K. , 1986: Instabilities. Mesoscale Meteorology and Forecasting, P. S. Ray, Ed., Amer. Meteor. Soc., 259-271.

Lester, P. F. and W. A. Fingerhut, 1974: Lower Turbulent Zones Associated with Mountain Lee Waves. J. Appl. Meteor. 13, 54-61.

MacCready, P. B., Jr., 1964: Standardization of gustiness values from aircraft. J. Appl. Meteor., 3, 439-449.

MacPherson, J. I., and G. A. Isaac, 1977: Turbulent characteristics of some Canadian cumulus clouds. J. Appl. Meteor., 16, 81-90.

McCann, D. W., 2001: Gravity waves, unbalanced flow, and aircraft clear air turbulence. Natl. Wea. Dig., 25, 3-14.

Miyakoshi, N. 2003: Turbulence indices using outer product of wind vector. Tenki, 50, 327-334.

Nakazawa, S., 2003: The common criteria for magnitude of turbulence in Japan airspace, METLINKSG/7-IP/13.

Obayashi, M., and S. Sakakibara, 2000: Aviation weather forecast. Text for NWP-training (*in Japanese, Suuchiyohou Kenshu Text*), Japan Meteorological Agency, 42-45.

Oono, H. and N. Miura, 1982: Excited Kelvin-Helmholtz billows just beneath the tropopause. Tenki, 29, 1235-1241.

Saito, K., and Coauthors, 2006: The Operational JMA Nonhydrostatic Mesoscale Model. Mon. Wea. Rev., 134, 1266-1298.

Saito, K., J. Ishida, K. Aranami, T. Hara, T. Segawa, M. Narita, and Y. Honda, 2007: Nonhydrostatic Atmospheric Models and Operational Development at JMA. J. Meteor. Soc. Japan, 85B, 271-304.

Scorer, R., 1949: Theory of waves in the lee of mountains. Quart. J. Roy. Meteor. Soc., 75, 41-56.

Sharman, R., C. Tebaldi, G. Wiener, and J. Wolff, 2006: An Integrated Approach to Mid- and Upper-Level Turbulence Forecasting, Weather and Forecasting, 21, 268-287.

Shen, B. and Y. Lin, 1999: Effects of Critical Levels on Two-Dimensional Back-Sheared Flow over an Isolated Mountain Ridge on an f Plane, J. Atmos. Sci., 56, 3286-3302.

Trier, S. D., R. D. Sharman, R. G. Fovell, and R. G. Frehlich, 2010: Numerical Simulation of Radial Cloud Bands within the Upper-Level Outflow of an Observed Mesoscale Convective System, J. Atmos. Sci., 67, 2990-2999.

Yamada. Y, 2008: Technical development for turbulence probability forecast. Note for aviation weather (*in Japanese, Kouku kishou note*). 1-11.

## Appendix A

### Newly developed turbulence diagnostics for candidates of explanatory variables

Turbulence is caused by various reasons besides KH instability. However, few indices are proposed for non-CAT turbulences. Therefore six diagnostics for mainly non-CAT turbulence are newly developed. The newly developed diagnostics are skew wind shear (SWS), convective cloud turbulence index (CONV), lee wave turbulence index (MTW1), vertically propagating mountain wave turbulence index (MTW2), mid-level cloud-base turbulence index (BASETB), and transverse band index (TRAV), in which SWS is an index intended for KH instability and the others for non-CAT turbulence. All new diagnostics are designed simply, so that they should be updated in the future. The effectiveness of newly developed indices is

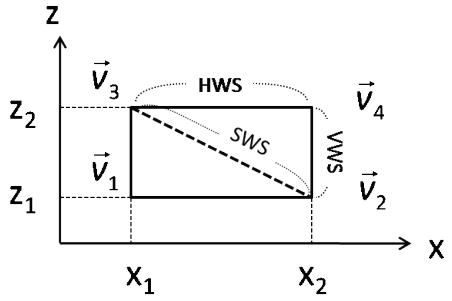


Fig. A1. A pattern diagram for VWS, HWS, and SWS. $\vec{v}$ indicates wind vector at each grid point, x and z indicate horizontal and vertical coordinate.

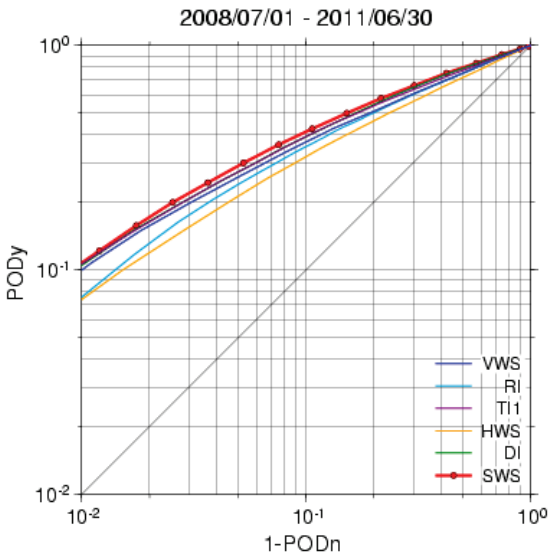


Fig. A2. PODy-PODn performance statistics for MOG turbulence for SWS, VWS, RI, TI1, HWS, and DI.

measured by the contribution to the regression equations (as shown in Table 2) and the forecast accuracy of TBindex.

*a. Skew Wind Shear (SWS)*

SWS is a wind shear calculated in a skew direction while VWS and HWS are a wind shear in a vertical and horizontal direction, respectively (Fig. A1). Because a grid point has multiple skew directions, SWS is defined as a length of "SWS vector" in this study,

$$\mathrm{SWS} = \sqrt{\mathrm{SWS_x}^2 + \mathrm{SWS_y}^2}$$

where SWSx and SWSy are averaged value of SWS in an east-west and north-south direction. Using the variables in Fig. A1, SWSx is defined as follows:

$$\mathrm{SWSx} = \frac{1}{2}\frac{|\vec{v}_3 - \vec{v}_2|}{z_2 - z_1} + \frac{1}{2}\frac{|\vec{v}_4 - \vec{v}_1|}{z_2 - z_1}$$

where horizontal and vertical intervals are set to 80 km and 2000 ft, respectively.

The key point in the definition of SWS is that the denominator is an altitude difference in a vertical direction while the numerator is a wind difference in a skew direction. There is no physical meaning for calculating wind shear in a skew direction but there is a meaning in terms of utilizing a NWP model output for the following reasons.

Turbulence via KH instability is generated by wind shears as an energy source. It is unlikely to be generated KH billows with a certain level of energy that affect aircraft by pure HWS because HWS is usually extremely weak compared to VWS in a common atmosphere (a typical value of HWS is about 10 kt/100km while that of VWS is about 10 kt/1000ft). In fact, the forecast accuracy of HWS is significantly low compared with VWS (see Fig. A2). However, some turbulence occur in the area where HWS is relatively large and VWS is relatively small (however, HWS is very small compared with VWS) in NWP models. It looks natural to understand that the turbulence occurs with locally strong VWS condition in large HWS area rather than the turbulence is generated by pure HWS. This is because if a gap is generated in the upper and lower flow for some reason in large HWS condition, large HWS is translated into large VWS which can cause turbulence. Therefore large HWS condition has a potential to be locally large VWS rather than small HWS condition. SWS is an index which presents a potential to be locally large VWS.

Figure 2A shows PODy-PODn (see Appendix B) performance statistics of SWS, VWS, RI, TI1, HWS, and DI for MOG turbulence. The verification period is three years from July 2008 to June 2011. C-PIREP is used for observation data. Verification results of forecast time from FT=4 to 15 and all forecast altitude are summed up in Fig. 2A. In the PODy-PODn diagram, lines located on near the upper-left corner have good performance. Though SWS is a simple index, the forecast accuracy is better than VWS and other indices as shown in Fig 2A.

*b. Convective cloud turbulence index (CONV)*

Turbulence is caused by a strong updraft and downdraft in convective clouds. In addition, if there is a large VWS layer in or top of the convective clouds, KH billows can be excited at the VWS layer by the strong updraft (Lane and Sharman 2008). A strong updraft and downdraft can be large with large updraft condition, and KH billows are easy to be exited with strong VWS and strong updraft condition. For these reasons, the convective cloud turbulence index is defined as follows:

$$\mathrm{CONV} = \mathrm{W_{mean}} \times \mathrm{VWS}$$

where $W_{mean}$ presents a mean updraft averaged in 40 km horizontal grid. $W_{mean}$ and VWS are a value at the grid point where CONV is calculated. If the mean updraft is negative (i.e. downdraft), CONV is treated as zero. In addition, in order to neglect an updraft without convective clouds, e.g. updraft with mountain waves, CONV is treated as zero in the case of before 1-hour precipitation amount is smaller than 1.0mm at the column.

*c. Lee wave turbulence index (MTW1)*

MTW1 is an index intended for turbulence in Lower Turbulent Zone (LTZ) (Lester and Fingerhut 1974) associated with mountain lee waves. Turbulence in LTZ is produced by the rotor or gusty wind in neutrally stable condition beneath a stable layer around mountain top height. The followings are points for forecasting turbulence in LTZ.

- Wind perpendicular to mountain ranges is relatively strong
- The atmospheric condition between the ground and a stable layer around mountain top height is nearly neutral
- Wind is relatively strong in the nearly neutral atmosphere

In accordance with the above points, MTW1 is calculated in the following procedure.

(1) A grid point with wind speed greater than 20 kt and the rate of vertical change of equivalence potential temperature less than 3 K/km between the ground and the lowest stable layer is searched.
(2) Next, A backward trajectory analysis from the grid point found in (1) as a start point up to four hours is performed. If the trajectory reaches a mountain range without protruding from the condition shown in (1), MTW1 at the start point is calculated as an inner product between a gradient of the surface altitude $z_s$ and a surface wind vector $\vec{v}_1(\mathrm{m/s})$ at the arrival point divided by $|\nabla z_s|$ and 10. MTW1 is defined as follows:

$$\mathrm{MTW1} = \frac{-\nabla z_s}{|\nabla z_s|} \cdot \frac{\vec{v}_1}{10}$$

In the case of $\mathrm{MTW1} \leq 1.5$, i.e. wind perpendicular to the mountain range is relatively weak, no mountain waves may occur, so that MTW1 is treated as 0. If the surface altitude of the mountain range is lower than 200 m in the NWP model, or the altitude difference between the mountain range and the start point is less than 100 m, MTW is treated as 0. MTW1 is smoothed around each grid after calculating MTW1 in every grid point.

*d. Vertically propagating mountain wave index* (MTW2)

Turbulence is generated by a break of vertically propagating mountain waves around critical levels or strong vertical wind shears (Gerbier and Berenger 1961; Shen and Lin 1999). Among then, turbulence with strong vertical wind shears can be presented by indices for KH instability, so that MTW2 is defined as an index intended for turbulence by a break of vertically propagating mountain waves around critical levels.

First, strong wind speed around the mountain top height is necessary for mountain wave generation. If the wind speed is strong, the incidence and intensity will be large. The critical level is a height at which the background wind speed becomes equal to the phase velocity. In the case of mountain waves, the phase velocity is nearly zero. To present these situations, MTW2 at a height z is defined as follows.

$$\mathrm{MTW2} = \frac{v_1 - v_2}{10}$$

where $v_1$ (kt) is wind speed at around the surface level, and $v_2$ (kt) is wind speed at a height z. if $v_1 \leq v_2$ or $v_1 \leq 30$ or surface altitude is lower than 200 m in the NWP model, MTW2 is treated as zero. MTW2 is smoothed around each grid after calculating MTW2 in every grid point. MTW2 becomes large when surface wind speed is strong and/or wind speed is weak at the upper level.

*e. Mid-level cloud-base turbulence index (BASETB)*

Turbulence can be caused by absolute instability beneath the mid-level cloud base resulting from sublimation cooling of snow (Kudo 2011). The followings are points for forecasting this kind of turbulence.

- There is an adequate amount of snow in the

atmosphere that does not reach the ground
- The humidity is low beneath the mid-level cloud base
- The temperature lapse rate beneath the cloud base is close to the dry adiabatic lapse rate
- Sublimation cooling of snow produces an absolutely unstable layer beneath the cloud base

The most important point is whether an absolute unstable layer is produced beneath the cloud base or not. Turbulence will occur when the absolute unstable layer is produced. In accordance with the above points, BASETB is calculated in the following procedure.

(1) First, the amount of solid precipitation that does not reach the ground is estimated for a column at which the before 1-hour precipitation is less than 0.5 mm. A grid point supersaturated with respect to ice is searched from the upper grid toward the lower side. If it is found, the extra mixing ratio is integrated toward the lower side until an unsaturated grid appears or the temperature becomes higher than 0°C.
(2) Next, temperature decrement beneath the cloud base by sublimation cooling of solid precipitation is estimated. If there is a grid unsaturated with respect to ice appears at the lower side of the supersaturated grid, the mixing ratio integrated in (1) is distributed with $(100 + \mathrm{Rh})/2$ as an upper limit until the integrated mixing ratio become zero or a supersaturated grid appears again. The temperature decrement $\Delta \mathrm{T}$ is derived from $\Delta \mathrm{T} = \mathrm{L}\,\Delta \mathrm{R_m}/\mathrm{C_p}$, where $\mathrm{L}$ is the latent heat of sublimation, $\Delta \mathrm{R_m}$ is the distributed mixing ratio, and $\mathrm{C_p}$ is the specific heat at constant pressure.
(3) Finally, temperature lapse rate $\Gamma$ (K/m) is calculated between the grid after cooling and the grid at one grid below before cooling. When the $\Gamma$ greater than the dry adiabatic lapse rate $\Gamma_\mathrm{d}$, BASETB is defined as follows:

$$\mathrm{BASETB} = \mathrm{Min}\big((\Gamma - \Gamma_\mathrm{d}) \times 1000, 1.0\big)$$

where the maximum value of BASETB is set 1.0, i.e. the maximum value of $\Gamma - \Gamma_\mathrm{d}$ is set 1.0 (K/km). This means, extremely large lapse rate cannot appear in the real atmosphere because the absolutely unstable layer can resolve relatively short time while solid precipitation sublimates gradually.

*f. Transverse band index (TRAV)*

Transverse bands are an important indicator of turbulence occurrence. Oono and Miura (1982) solved a one-dimensional structural equation with typical profiles of temperature and wind in the equator side of jet streams by numerical calculation. As a result, they concluded that transverse bands are KH billows exited in the low stability layer beneath a tropopause. The occurrence conditions are: the thickness of a low stability layer exceed 1 km, Richardson number is nearly 0.25 or less, and the maximum wind speed in the jet stream exceeds 50 m/s (～100 kt). However in the real atmosphere, transverse bands seem to appear around a tropopause located above a low stability layer in the equator side of jet streams with wind speed exceeds about 100 kt and VWS is slightly large. In order to present these points, TRAV is calculated in the following procedure.

(1) First, a layer with wind speed exceeds 100 kt and the rate of vertical change of equivalent potential temperature less than 2.0 K/km is searched from the lower layer toward the upper side.
(2) If there is a grid point with wind speed exceeds 100 kt and the rate of vertical change of equivalent potential temperature greater than 2.0 K/km in 4000 ft above the layer searched in (1), TRAV is VWS at the grid.

TRAV become large when VWS is large above a low stability layer with wind speed exceeds 100 kt.

## Appendix B

## Verification scores

Verification scores using in this paper are shown. Each variable using in the followings is defined in Table A1.

Table A1. 2x2 contingency table.

| Forecast | Observed | |
|---|---|---|
| | Yes | No |
| Yes | a | b |
| No | c | d |

*a. Hit Rate (Hr, PODy)*

The Hit Rate (or probability of detection yes events) is the fraction of correct forecast in yes observation. It is calculated as follows:

$$\mathrm{PODy} = \frac{\mathrm{a}}{\mathrm{a} + \mathrm{c}}$$

It ranges from 0 (poor) to 1 (good).

*b. False Alarm Rate (Fr, PODn)*

The False Alarm Rate (or probability of detection no events) is the fraction of wrong forecast in no observation. It is calculated as follows:

$$\mathrm{PODn} = \frac{\mathrm{b}}{\mathrm{b} + \mathrm{d}}$$

It ranges from 0 (good) to 1 (poor).

*c. Heidke Skill Score (HSS)*

The Heidke Skill Score is a percent correct except for the correct by random forecasts. It is calculated as follows:

$$\mathrm{HSS} = \frac{2(\mathrm{ad} - \mathrm{bc})}{(\mathrm{a} + \mathrm{c})(\mathrm{c} + \mathrm{d}) + (\mathrm{a} + \mathrm{b})(\mathrm{b} + \mathrm{d})}$$

It ranges from $-1$ (worst) to 1 (best), and HSS=0 means a random forecast.